"ARDS and Cytokine Storm in SARS-CoV-2 Infected Caribbean Vervets"

[1]Robert V. Blair, [1]Monica Vaccari, [1]Lara A. Doyle-Meyers, [1]Chad J Roy, [1]Kasi Russell-Lodrigue, [1]Marissa Fahlberg, [1]Chris J. Monjure, [1,2]Brandon Beddingfield, [3]Kenneth S. Plante, [3]Jessica A. Plante, [3]Scott C. Weaver, [1]Xuebin Qin, [1]Cecily C. Midkiff, [1]Gabrielle Lehmicke, [1]Nadia Golden, [1]Breanna Threeton, [1]Toni Penney, [1]Carolina Allers, [1]Mary B Barnes, [1]Melissa Pattison, [1]Prasun K Datta, [1]Nicholas J Maness, [1]Angela Birnbaum, [1]Tracy Fischer, [1]Rudolf P. Bohm, *[1]Jay Rappaport

[1]Tulane National Primate Research Center, Covington, LA

[2]Tulane University School of Medicine, Department of Microbiology and Immunology, New Orleans, LA

[3] World Reference Center for Emerging Viruses and Arboviruses, Institute for Human Infections and Immunity, University of Texas Medical Branch, Galveston, TX

*To whom correspondence should be addressed:

Jay Rappaport, Ph.D.

Director and Chief Academic Officer

Tulane National Primate Research Center

18703 Three Rivers Road, Covington, LA 70433

Tel. 985-871-6201

Fax. 985871, 6569

Abstract

SARS-CoV-2 induces a wide range of disease severity ranging from asymptomatic infection, to a life-threating illness, particularly in the elderly and persons with comorbid conditions. Up to now, SARS-CoV-2 has infected more than five million and led to more than 300,000 deaths worldwide. Among those persons with serious COVID-19 disease, acute respiratory distress syndrome (ARDS) is a common and often fatal presentation. SARS-CoV-2-induced ARDS is difficult to treat clinically, and new therapeutic strategies are needed. In order to evaluate such therapeutic strategies, animal models of SARS-CoV-2 infection that manifest severe disease are needed. Here we report fatal ARDS in two African green monkeys (AGMs) infected with SARS-CoV-2 that demonstrated pathological lesions and disease similar to severe COVID-19 in humans. Moreover, we report the observation of cytokine release (cytokine storm) in three of four infected AGMs. All four animals showed increased levels of IL-6 in plasma, a predictive marker and presumptive therapeutic target in humans infected with SARS-CoV-2 infection. Our results suggest the AGM is a useful model to study disease pathogenesis of SARS-CoV-2, and for the evaluation of therapeutic interventions designed to combat serious pulmonary disease associated with this infection.

The coronavirus disease-2019 (COVID-19) pandemic, caused by the novel coronavirus, severe acute respiratory syndrome coronavirus-2 (SARS-CoV-2), has resulted in the deaths of hundreds of thousands of people and has caused massive economic and health disruptions across the globe. This unprecedented level of disruption has been driven by two main features of SARS-CoV-2: its high rate of person-to-person transmissibility and the potential to cause severe, life-threatening, pneumonia. Although severe disease is only seen in a small subset of infected people[1], it is this outcome and minimal understanding of its pathogenesis that has resulted in global unrest. Research into the causes and mechanisms of the most severe manifestations of COVID-19 is needed to inform and facilitate the development of prophylactic and therapeutic approaches that can prevent this life-threatening outcome.

Infection with SARS-CoV-2 and development of COVID-19 results in a mild respiratory disease for most individuals. However, a small subset progress to develop severe respiratory disease which in some cases is fatal[1]. The most severely affected individuals often present with a fever, cough, dyspnea, and bilateral radiographic opacities that in the majority of critically ill patients progresses to acute respiratory distress syndrome (ARDS)[2]. The onset of ARDS is often associated with an increase in circulating pro-inflammatory cytokines resulting in a cytokine release syndrome colloquially referred to as a "cytokine storm"[3,4]. Interleukin-6 (IL-6), in particular has been shown to correlate with radiographic scores in patients with SARS-CoV-2 infection[5]. Worsening of disease can be seen in the context of declining viral loads and markedly elevated cytokines suggesting a role for these inflammatory responses in disease progression and immunopathology[6]. Despite extensive research during both the SARS-CoV and the Middle East respiratory syndrome (MERS) outbreaks, the factors that drive this inflammatory response are still poorly understood.

Animal models have been used extensively during previous outbreaks of SARS-CoV[7-10] and MERS[11-13] to model disease progression and to test vaccines and therapeutics[14]. Nonhuman primates (NHPs) are ideally suited to model respiratory human viral infections primarily because of the similarities in respiratory anatomy and immunologic responses when compared to other animal species. Several NHP species have been used in the past to model infections with both SARS-CoV and MERS including marmosets (*Callithrix jacchus*) [10,12,15], rhesus macaques (*Macaca mulatta*)[12,13,16,17], cynomolgus macaques (*Macaca fascicularis*)[7,8,17], and African green monkeys (*Chlorocebus aethiops*)[8,9,17]. All these species have been shown to be susceptible to infection with these viruses and develop mild to moderate disease, but none have been able to recapitulate the rapid clinical deterioration seen in people with severe disease and ARDS. NHP models capable of recapitulating the entire spectrum of SARS-CoV-2 manifestations, from mild to severe disease, are urgently needed to test the efficacy of vaccines and medical countermeasures that are currently being developed in response to COVID-19.

Here we report the sudden and rapid health deterioration of two out of four AGMs experimentally infected with SARS-CoV-2. The two effected animals developed pneumonia, ARDS and a cytokine storm similar to the complications reported in 5-13% of COVID-19 patients[18].

ARDS in SARS-CoV-2 infected AGMs

Four, aged, AGMs were exposed by two routes to SARS-CoV-2 isolate USA-WA1/2020. Two animals were exposed via small particle aerosol (AGM1, AGM4) resulting in an inhaled dose of $2.0x10^3$ and $2.5x10^3$ PFU, respectively. Two AGMs were exposed via multiple route installation (AGM 2, AGM3) including conjunctival, intratracheal, oral, and intranasal exposure resulting in a cumulative dose of $3.61x10^6$ PFU (Extended Data Table 1). SARS-CoV-2 was detectable in swabs obtained from mucosal sites in all four animals. Viral load peaked between 3- and 7- days post inoculation (DPI) and persisted throughout the course of the study in pharyngeal and nasal swabs as well as bronchial brush samples (Figure 1). The highest levels of virus were detected in the pharynx and nasal cavity with peaks at 10^7-10^{11} and 10^8-10^9 copies per swab, respectively. Rectal swabs contained high viral load similar to reports in humans[19,20]; however, with dissimilar kinetics relative to virus detected in other sites. Virus was also detected in vaginal swabs of the two female AGMs in contrast to reports in human subjects[21]. Despite the three-log difference in exposure dose, no significant difference was observed in the viral load or kinetics when the two routes of exposure were compared.

After SARS-CoV-2 exposure, animals were followed up to four weeks post-infection with regular clinical assessment that included physical exam, pulse oximetry, and plethysmography. Clinical findings during the first 6 DPI included mild transient changes in SpO_2 and appetite (Extended Data Figure 1). At 7 DPI all animals underwent a complete physical evaluation and an extensive sample collection protocol including fluid (urine, CSF, BAL, and vaginal and rectal weks), stool, swab (buccal, nasal, and pharyngeal), and bronchial brush collection, no remarkable findings were noted. That afternoon (7 DPI), AGM1 developed mild tachypnea that progressed to severe respiratory distress in less than 24 hours. On the morning of the 8 DPI, the animal was discovered recumbent and exam findings included dyspnea, tachypnea, hypothermia, and an

SpO_2 of 77% under oxygen supplementation (Extended Data Figure 1c, e, f). This differed from reports of critically ill SARS-CoV-2 patients which often present with fever in addition to dyspnea[2]. On 21 DPI the three remaining animals underwent another complete evaluation. During the morning exam on 22 DPI, AGM2 began exhibiting tachypnea that progressed to severe respiratory distress by that afternoon. The onset, clinical presentation, and rate of progression of disease in AGM2 was similar to AGM1 and included dyspnea, tachypnea, hypothermia, and a $Sp0_2$ of 77% on ambient air.

Thoracic radiographs for AGM1 and AGM2 revealed a diffuse alveolar pattern of disease throughout the right lung fields and a lobar sign in the caudal dorsal lung field. These findings were in stark contrast to the radiographs from the day before (Figure 2a, b). CBC showed an elevated WBC with a mature neutrophilia and a normal lymphocyte count that resulted in an elevated neutrophil-to-lymphocyte ratio (NLR) (Extended Data 2a, f). Serum chemistries revealed hypoproteinemia, and an elevated glucose and mild to moderate elevation in BUN for both animals. Creatinine, and AST were also mildly elevated in AGM1 (Extended Data Figure 3a, d-f, h). The radiographic presentation in severe human COVID-19 is similar and characterized by bilateral, peripheral, ill-defined ground glass opacifications that mainly involve the right lower lobe[22]. An elevation in the NLR has been identified as an independent risk factor for mortality in hospitalized patients with SARS-CoV-2, and increased NLR significantly correlated with elevations in AST, glucose, BUN, and creatinine in these patients[23]. The constellation of hematologic changes in AGM1 and AGM2 is therefore similar to the changes observed in human COVID-19 patients with increased NLR; however in humans, increased NLR is often associated with lymphopenia[24] which was not observed in these two animals.

Due to their rapidly declining clinical condition AGM1 and AGM2 were euthanized and a necropsy was performed at 8 and 22 DPI, respectively. The two remaining animals, AGM3 and AGM4 (multiroute and aerosol exposure respectively) reached the study endpoint with no significant changes in clinical parameters.

Cytokine storm in two AGMs with, and one without, ARDS

Cytokine release syndrome has been observed in a subgroup of patients with severe COVID-19 pneumonia[25]. In these patients the disease progresses rapidly, and mortality is high. A panel of cytokines was measured in plasma at baseline and during the course of infection. Interferon gamma (IFNγ) responses increased at 1 week post infection in all animals as shown by the heat map and the radial plot in Figure 3a, b. IFNγ levels were higher in AGM1 and AGM2 and were associated with viral RNA in the bronchial brushes at the same time point (1 week) (Figure 3c, d).

A group of cytokines similar to what is observed in human COVID-19 was upregulated in AGM1 and AGM2 at the time of necropsy compared to baseline levels in the two animals that progressed to ARDS (Figure 3a, b). Elevated markers included IL-6, IL-4/IL-13, IL-8, IL-1β and TNFα consistent with cytokine storm. AGM3 and AGM4 did not develop ARDS; however, AGM4 showed increased cytokine concentrations and evidence of cytokine storm. AGM3 had

increased levels of IL-10 both at week 1 and necropsy and was notable for having the least severe disease of the group.

Absence of SARS-CoV-2 antibody titers in animals with ARDS

Binding IgG antibody to S1 and S2 subunits of the spike protein (Wuhan-Hu 1 strain) were measured at pre-infection and terminally for all animals by ELISA. Antibodies were not detected prior to infection in any of the animals used in this infection study. Antibodies remained undetectable in the 2 animals that progressed to ARDS (AGM1, 8 DPI; AGM2, DPI). Both animals that survived to the end of the study with no observable clinical disease had detectable circulating antibodies (Extended Data Figure 5).

Pulmonary pathology in AGMs with ARDS

Gross postmortem examination of AGM1 and AGM2 revealed severe consolidation and edema in the right caudal lung lobe with generalized failure to collapse of the remaining lobes, consistent with a bronchointerstitial pneumonia (Figure 2c, d). In AGM2 (multiroute exposure) pulmonary hemorrhage was also noted near the dorsal margin of the right caudal lung lobe. AGM3 had multifocal pleural adhesions between the left caudal lung lobe and the diaphragm that was interpreted as being unrelated to SARS-CoV-2 infection based on the chronicity of the lesion and the history of the animal. The lungs of AGM4 were grossly normal. No significant abnormalities were noted outside the pulmonary changes in any of the four AGMs.

Histopathologic findings in AGM1 and AGM2 were similar and characterized by alveoli that were filled with fibrin, hemorrhage, and proteinaceous fluid. Alveoli were multifocally lined by hyaline membranes and/or type II pneumocytes, consistent with diffuse alveolar damage. Bronchial and alveolar septal necrosis were present within severely affected lung lobes characterized by a loss of epithelial lining cells and infiltration by neutrophils with lesser numbers of lymphocytes and histiocytes (Figure 4a, b). In AGM1, type II pneumocytes frequently exhibited atypia and occasionally contained mitotic figures. Regions of the lung from AGM1 also had organization of intra-alveolar fibrin with infiltration by spindle cells and lining by type II pneumocytes, consistent with early organizing pneumonia. Low numbers of multinucleated giant cell syncytia were scattered throughout alveoli (Figure 4c). Fluorescent immunohistochemistry identified low numbers of type II pneumocytes and alveolar macrophages that were positive for SARS-CoV-2 nucleoprotein within the affected lungs from AGM1, but not AGM2. (Figure 4d). AGM4 had multifocal, mild to moderate, interstitial pneumonia scattered throughout all lung lobes characterized by a mixed infiltrate of neutrophils, lymphocytes, and histiocytes. Multinucleated giant cell syncytia and atypical pneumocyte hyperplasia were rarely observed in all lung lobes. AGM3 had scant inflammation in all lung lobes examined. Viral load was not significantly associated with pulmonary pathology; however, the two animals that developed diffuse alveolar damage showed higher viral loads in bronchi.

Discussion

Exposure of African green monkeys to SARS-CoV-2 resulted in the development of spontaneous ARDS in two of four animals studied. Although severe pathologic changes have been described in AGMs euthanized at early time points post infection[8], the rapid clinical decline with

progression to ARDS seen in the most severe cases of COVID -19 patients has not been reported in NHP models [9,17,26]. Our findings show that AGMs are capable of recapitulating the severe disease manifestations seen in people, both at the pathological and immunological level.

Several predisposing conditions are known to increase the likelihood of developing severe disease in people following infection with SARS-CoV-2. Age[2], weight[27], and sex[2,28] at one point have been identified as potential predisposing factors for developing severe disease. All of the AGMs included in our study were aged, with an estimated age of 16 years old, which may explain why prior studies using AGMs to model respiratory coronavirus infections have not shown the ARDS-phenotype observed in our study. Both animals that progressed to severe disease were female and low weight. This differs from what is reported in COVID-19 patients in which male gender[29,30] and obesity[27] have been shown to have a higher prevalence of severe disease.

There are animal characteristics that may have influenced the outcome of this study. The AGMs used in this infection study were imported from nondomestic sources. Detailed longitudinal information usually available in domestic breeding colonies (*e.g.* medical history, housing, diet) was not available. All animals used on the study were found to be in excellent health upon importation and underwent an unremarkable 90-day quarantine period prior to use. All animals were examined, and screened for viral, bacterial, and parasitic infections prior to inclusion as subjects on this study. Although the animals were deemed clinically healthy at the time of initiation of the study, there may have been historical factors that predisposed them to enhanced COVID-19 disease.

The pathogenesis of ARDS is still poorly understood. ARDS has multiple causes and several animal models have been utilized in the past to study this syndrome. These include models of sepsis, hyperoxia, aerosolized toxin[31], and acid aspiration[32]. These models have highlighted the importance of the innate host immune response in the development of acute lung injury. Proinflammatory cytokines including TNFα, IL-1β, IL-8, IL-6, G-CSF, MCP-1, and MIP-1 have been shown to be elevated during the acute phases of acute lung injury (ALI)[33]. Indeed, overexpression of several of these cytokines were observed in both animals that progressed to ARDS. This differed from the cytokine profile in the animals that reached study endpoint. Of these animals, only a few cytokines (IL-6, IL-8 and IL-10) were elevated in AGM3; whereas, AGM4 exhibited an intermediate phenotype with increased levels of several cytokines (IL-1β, TNFα, IL-8, IL-13, and IL-4 but not IL-10). Interestingly, at 7 DPI all four animals had increased levels of IFNγ, with the two progressors having the highest plasma concentration. The IFNγ plasma levels at 7 DPI were positively associated with viral load in bronchial brush samples at the same time ($p=0.015$, $R=0.99$, Pearson test) suggesting that viral load may be driving the IFNγ response. Some groups have proposed that IFNγ production maybe favorable to the virus through upregulation of ACE2 from IFNγ stimulation[34]. Thus, elevated IFNγ in plasma could be explored as a potential biomarker for advanced disease in people.

In human COVID-19, circulating IL-6 correlates with radiographic abnormalities of pneumonia[3], and was found to be upregulated in both animals that progressed to ARDS and also elevated in the animals without ARDS, albeit to a lesser degree (Figure 3b). Immunohistochemistry

identified low numbers of virally infected cells localized in multifocal clusters. The localized distribution taken together with the widespread pathology, and the lack of detectable virus by IHC in one of the two AGMs that progressed to ARDS, suggests that the development of ARDS may not be due to direct viral effects and highlights the potential importance of cytokine storm in ARDS progression in these two animals.

Previous studies on SARS-CoV have shown the protective effects of neutralizing antibodies in immunized animal models[35-37]. No data is yet available on the role of non-neutralizing binding antibodies in disease progression; however, it is interesting to note that neither of the progressors had detectable spike (S) specific IgG antibodies at the terminal time point. This is in stark contrast to both surviving AGMs that had circulating anti-S IgG antibodies. The terminal sample from AGM1 was acquired 8 DPI which may have been too early to demonstrate an IgG-type response. But, the sample from AGM2 was acquired at 22 DPI and therefore an antibody response would have been expected based on the timing of the responses in AGMs 3 and 4 (without disease). Further investigation is needed to determine if these antibodies were neutralizing, and the mechanisms underlying the restricted antibody response observed in the two progressors.

The clinical progression in both animals was fulminant, and neither animal demonstrated significant abnormalities on any of our diagnostic assays until the day of their progression. This emphasizes the need for the development of better diagnostic tests that can more accurately predict disease outcome. Animal models are ideally suited for these types of investigational studies where infection takes place in a controlled setting, and repeated, longitudinal sampling can occur at key acute time points. Identification of early clinical and immunological biomarkers that are predictive of mortality and disease severity will also facilitate disease management.

This study demonstrates that following exposure to SARS-CoV-2 AGMs develop a spectrum of disease, from mild to severe COVID-19, which in some cases progress to ARDS. The cytokine expression profile in the two animals that developed ARDS is similar to the severe disease phenotype in people. Exploratory disease model development plays a crucial role in elucidating the early pathogenic mechanisms and predictors of disease outcome for emerging infectious diseases like SARS-CoV-2.

1 Wu, Z. & McGoogan, J. M. Characteristics of and Important Lessons From the Coronavirus Disease 2019 (COVID-19) Outbreak in China: Summary of a Report of 72314 Cases From the Chinese Center for Disease Control and Prevention. *JAMA*, doi:10.1001/jama.2020.2648 (2020).

2 Yang, X. *et al.* Clinical course and outcomes of critically ill patients with SARS-CoV-2 pneumonia in Wuhan, China: a single-centered, retrospective, observational study. *Lancet Respir Med* **8**, 475-481, doi:10.1016/S2213-2600(20)30079-5 (2020).

3 Chien, J. Y., Hsueh, P. R., Cheng, W. C., Yu, C. J. & Yang, P. C. Temporal changes in cytokine/chemokine profiles and pulmonary involvement in severe acute respiratory syndrome. *Respirology* **11**, 715-722, doi:10.1111/j.1440-1843.2006.00942.x (2006).

4 Channappanavar, R. & Perlman, S. Pathogenic human coronavirus infections: causes and consequences of cytokine storm and immunopathology. *Semin Immunopathol* **39**, 529-539, doi:10.1007/s00281-017-0629-x (2017).

5 McGonagle, D., Sharif, K., O'Regan, A. & Bridgewood, C. The Role of Cytokines including Interleukin-6 in COVID-19 induced Pneumonia and Macrophage Activation Syndrome-Like Disease. *Autoimmun Rev* **19**, 102537, doi:10.1016/j.autrev.2020.102537 (2020).

6 Weiss, S. R. & Leibowitz, J. L. Coronavirus pathogenesis. *Adv Virus Res* **81**, 85-164, doi:10.1016/B978-0-12-385885-6.00009-2 (2011).

7 Lawler, J. V. *et al.* Cynomolgus macaque as an animal model for severe acute respiratory syndrome. *PLoS medicine* **3**, e149, doi:10.1371/journal.pmed.0030149 (2006).

8 Smits, S. L. *et al.* Distinct severe acute respiratory syndrome coronavirus-induced acute lung injury pathways in two different nonhuman primate species. *Journal of virology* **85**, 4234-4245, doi:10.1128/JVI.02395-10 (2011).

9 Clay, C. C. *et al.* Severe acute respiratory syndrome-coronavirus infection in aged nonhuman primates is associated with modulated pulmonary and systemic immune responses. *Immun Ageing* **11**, 4, doi:10.1186/1742-4933-11-4 (2014).

10 Greenough, T. C. *et al.* Pneumonitis and multi-organ system disease in common marmosets (Callithrix jacchus) infected with the severe acute respiratory syndrome-associated coronavirus. *The American journal of pathology* **167**, 455-463, doi:10.1016/S0002-9440(10)62989-6 (2005).

11 Yeung, M. L. *et al.* MERS coronavirus induces apoptosis in kidney and lung by upregulating Smad7 and FGF2. *Nat Microbiol* **1**, 16004, doi:10.1038/nmicrobiol.2016.4 (2016).

12 Baseler, L. J. *et al.* An Acute Immune Response to Middle East Respiratory Syndrome Coronavirus Replication Contributes to Viral Pathogenicity. *The American journal of pathology* **186**, 630-638, doi:10.1016/j.ajpath.2015.10.025 (2016).

13 de Wit, E. *et al.* Prophylactic and therapeutic remdesivir (GS-5734) treatment in the rhesus macaque model of MERS-CoV infection. *Proceedings of the National Academy of Sciences of the United States of America* **117**, 6771-6776, doi:10.1073/pnas.1922083117 (2020).

14 Datta, P. K. L., F; Fischer, T; Rappaport, J; and Qin, X. SARS-CoV-2 pandemic and research gaps: Understanding SARS-CoV-2 interaction with the ACE2 receptor and implications for therapy. *Theranostics*, doi:10.7150/thno.48076 (2020).

15 Chan, J. F. *et al.* Treatment With Lopinavir/Ritonavir or Interferon-beta1b Improves Outcome of MERS-CoV Infection in a Nonhuman Primate Model of Common Marmoset. *The Journal of infectious diseases* **212**, 1904-1913, doi:10.1093/infdis/jiv392 (2015).

16 Lan, J. *et al.* Recombinant Receptor Binding Domain Protein Induces Partial Protective Immunity in Rhesus Macaques Against Middle East Respiratory Syndrome Coronavirus Challenge. *EBioMedicine* **2**, 1438-1446, doi:10.1016/j.ebiom.2015.08.031 (2015).

17 McAuliffe, J. *et al.* Replication of SARS coronavirus administered into the respiratory tract of African Green, rhesus and cynomolgus monkeys. *Virology* **330**, 8-15, doi:10.1016/j.virol.2004.09.030 (2004).

18 Hu, Y. *et al.* Prevalence and severity of corona virus disease 2019 (COVID-19): A systematic review and meta-analysis. *J Clin Virol* **127**, 104371, doi:10.1016/j.jcv.2020.104371 (2020).

19 Wang, W. *et al.* Detection of SARS-CoV-2 in Different Types of Clinical Specimens. *JAMA*, doi:10.1001/jama.2020.3786 (2020).

20 To, K. K. *et al.* Temporal profiles of viral load in posterior oropharyngeal saliva samples and serum antibody responses during infection by SARS-CoV-2: an observational cohort study. *Lancet Infect Dis* **20**, 565-574, doi:10.1016/S1473-3099(20)30196-1 (2020).

21 Qiu, L. *et al.* SARS-CoV-2 is not detectable in the vaginal fluid of women with severe COVID-19 infection. *Clinical infectious diseases : an official publication of the Infectious Diseases Society of America*, doi:10.1093/cid/ciaa375 (2020).

22 Shi, H. *et al.* Radiological findings from 81 patients with COVID-19 pneumonia in Wuhan, China: a descriptive study. *Lancet Infect Dis* **20**, 425-434, doi:10.1016/S1473-3099(20)30086-4 (2020).

23 Liu, Y. *et al.* Neutrophil-to-lymphocyte ratio as an independent risk factor for mortality in hospitalized patients with COVID-19. *J Infect*, doi:10.1016/j.jinf.2020.04.002 (2020).

24 Fan, B. E. *et al.* Hematologic parameters in patients with COVID-19 infection. *Am J Hematol* **95**, E131-E134, doi:10.1002/ajh.25774 (2020).

25 Huang, C. *et al.* Clinical features of patients infected with 2019 novel coronavirus in Wuhan, China. *Lancet* **395**, 497-506, doi:10.1016/S0140-6736(20)30183-5 (2020).

26 Clay, C. *et al.* Primary severe acute respiratory syndrome coronavirus infection limits replication but not lung inflammation upon homologous rechallenge. *Journal of virology* **86**, 4234-4244, doi:10.1128/JVI.06791-11 (2012).

27 Simonnet, A. *et al.* High prevalence of obesity in severe acute respiratory syndrome coronavirus-2 (SARS-CoV-2) requiring invasive mechanical ventilation. *Obesity (Silver Spring)*, doi:10.1002/oby.22831 (2020).

28 Walter, L. A. & McGregor, A. J. Sex- and Gender-specific Observations and Implications for COVID-19. *West J Emerg Med*, doi:10.5811/westjem.2020.4.47536 (2020).

29 Jin, J. M. *et al.* Gender Differences in Patients With COVID-19: Focus on Severity and Mortality. *Front Public Health* **8**, 152, doi:10.3389/fpubh.2020.00152 (2020).

30 Dudley, J. P. & Lee, N. T. Disparities in Age-Specific Morbidity and Mortality from SARS-CoV-2 in China and the Republic of Korea. *Clinical infectious diseases : an official publication of the Infectious Diseases Society of America*, doi:10.1093/cid/ciaa354 (2020).

31 Roy, C. J. *et al.* Rescue of rhesus macaques from the lethality of aerosolized ricin toxin. *JCI insight* **4**, doi:10.1172/jci.insight.124771 (2019).

32 Matute-Bello, G., Frevert, C. W. & Martin, T. R. Animal models of acute lung injury. *Am J Physiol Lung Cell Mol Physiol* **295**, L379-399, doi:10.1152/ajplung.00010.2008 (2008).

33 O'Grady, N. P. *et al.* Local inflammatory responses following bronchial endotoxin instillation in humans. *Am J Respir Crit Care Med* **163**, 1591-1598, doi:10.1164/ajrccm.163.7.2009111 (2001).

34 Ziegler, C. G. K. *et al.* SARS-CoV-2 Receptor ACE2 Is an Interferon-Stimulated Gene in Human Airway Epithelial Cells and Is Detected in Specific Cell Subsets across Tissues. *Cell*, doi:10.1016/j.cell.2020.04.035 (2020).

35 Yang, Z. Y. *et al.* A DNA vaccine induces SARS coronavirus neutralization and protective immunity in mice. *Nature* **428**, 561-564, doi:10.1038/nature02463 (2004).

36 Bukreyev, A. *et al.* Mucosal immunisation of African green monkeys (Cercopithecus aethiops) with an attenuated parainfluenza virus expressing the SARS coronavirus spike protein for the prevention of SARS. *Lancet* **363**, 2122-2127, doi:10.1016/S0140-6736(04)16501-X (2004).

37 Qin, E. *et al.* Immunogenicity and protective efficacy in monkeys of purified inactivated Vero-cell SARS vaccine. *Vaccine* **24**, 1028-1034, doi:10.1016/j.vaccine.2005.06.038 (2006).

38 Hartings, J. M. & Roy, C. J. The automated bioaerosol exposure system: preclinical platform development and a respiratory dosimetry application with nonhuman primates. *J Pharmacol Toxicol Methods* **49**, 39-55, doi:10.1016/j.vascn.2003.07.001 (2004).

39 Kolde, R. pheatmap: Pretty Heatmaps. *R package version 1.0.12* (2018).

40 Team, R. C. R: A language and environment for statistical computing. *R Foundation for Statistical Computing* (2019).

41 Wickham, H. ggplot2: Elegant Graphics for Data Analysis. (2016).

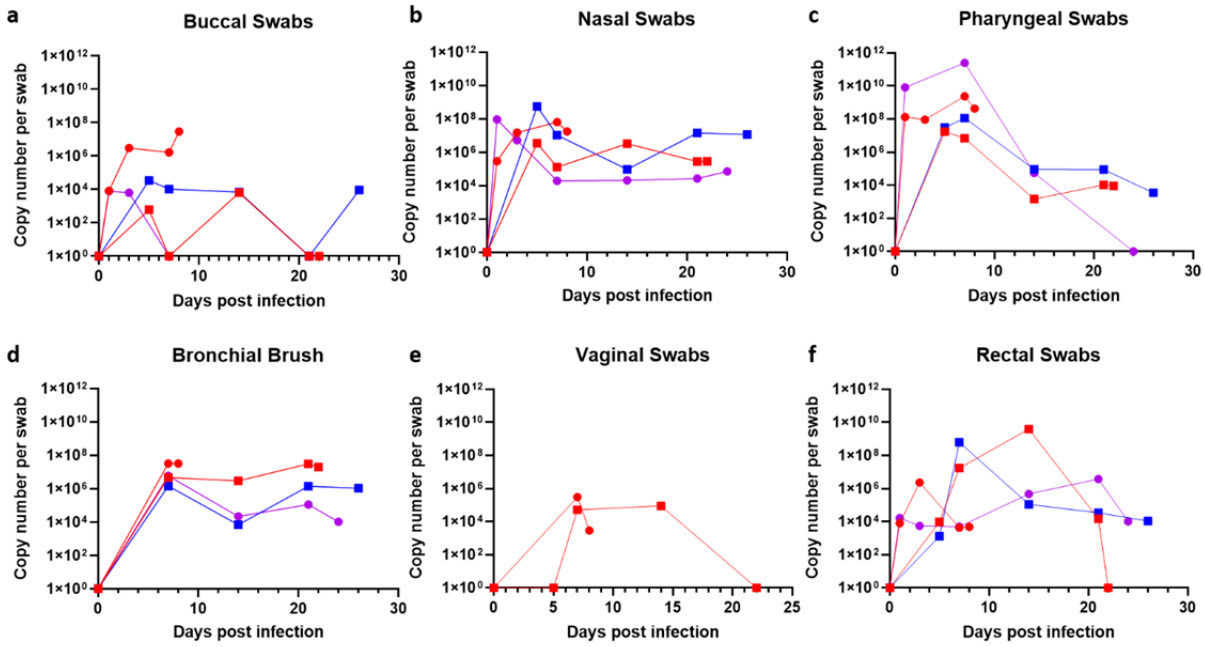

Figure 1 | Quantification of viral loads from mucosal swabs. All four African green monkeys had detectable virus at all mucosal sites. No significant differences were noted between viral load and route of exposure. Animals with pathology trended to high viral loads in bronchial brush samples. Circles: aerosol exposure; Squares: multiroute exposure; Red: developed ARDS; Purple: cytokine storm without ARDS; Blue: no cytokine storm or ARDS.

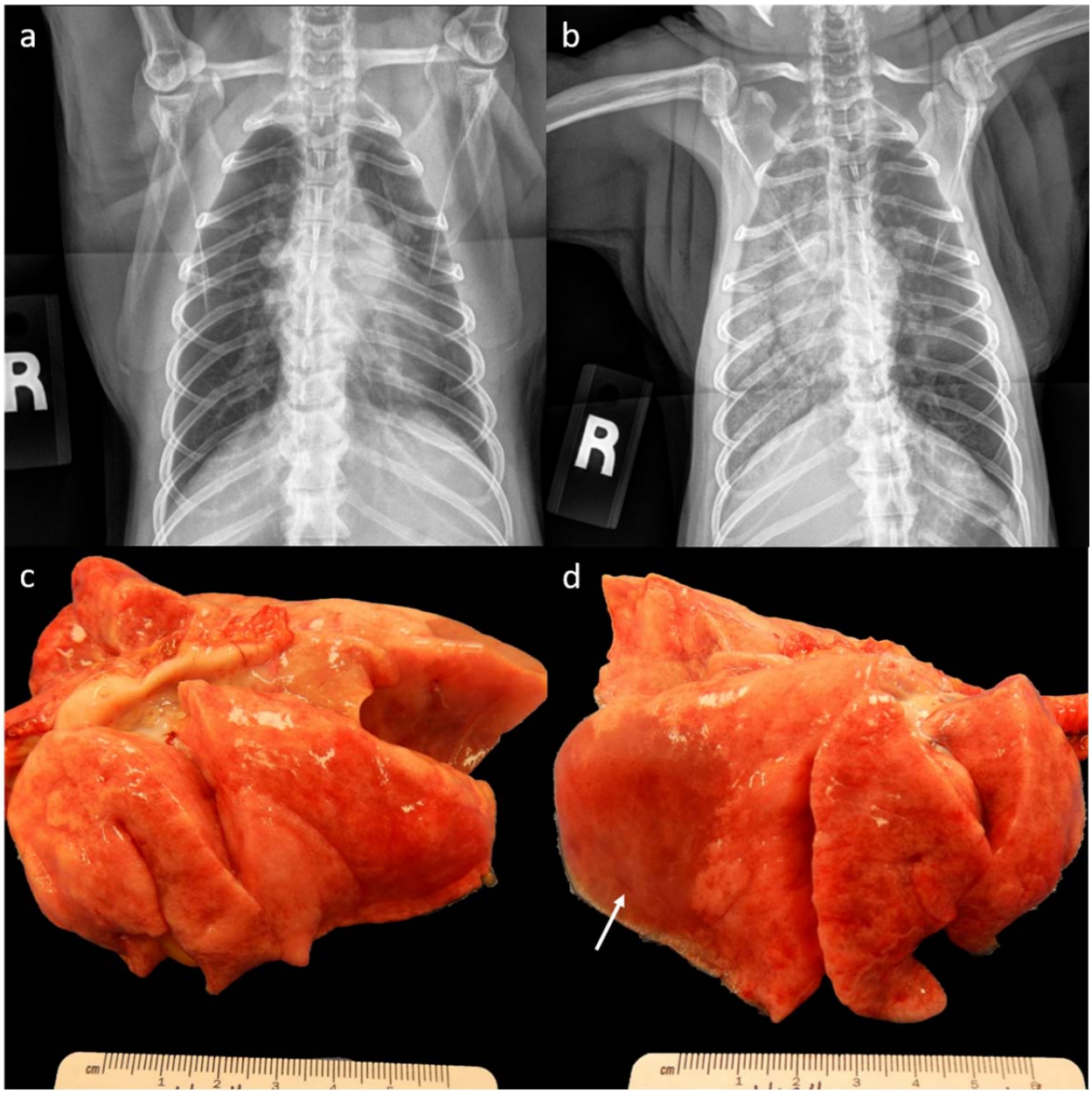

Figure 2 | Radiographic and gross pathologic changes in CoV-2 exposed African green monkey, AGM1. Radiographs 22 hours before (a) and at the time of necropsy (b) showing the rapid development of alveolar lung opacities throughout the right lung lobes. (c) The left lung lobes fail to collapse. (d) There is extensive consolidation of the right lower lung lobe with pulmonary edema (arrow). The right middle and anterior lobes are less affected. On cut surface all lobes ooze copious fluid.

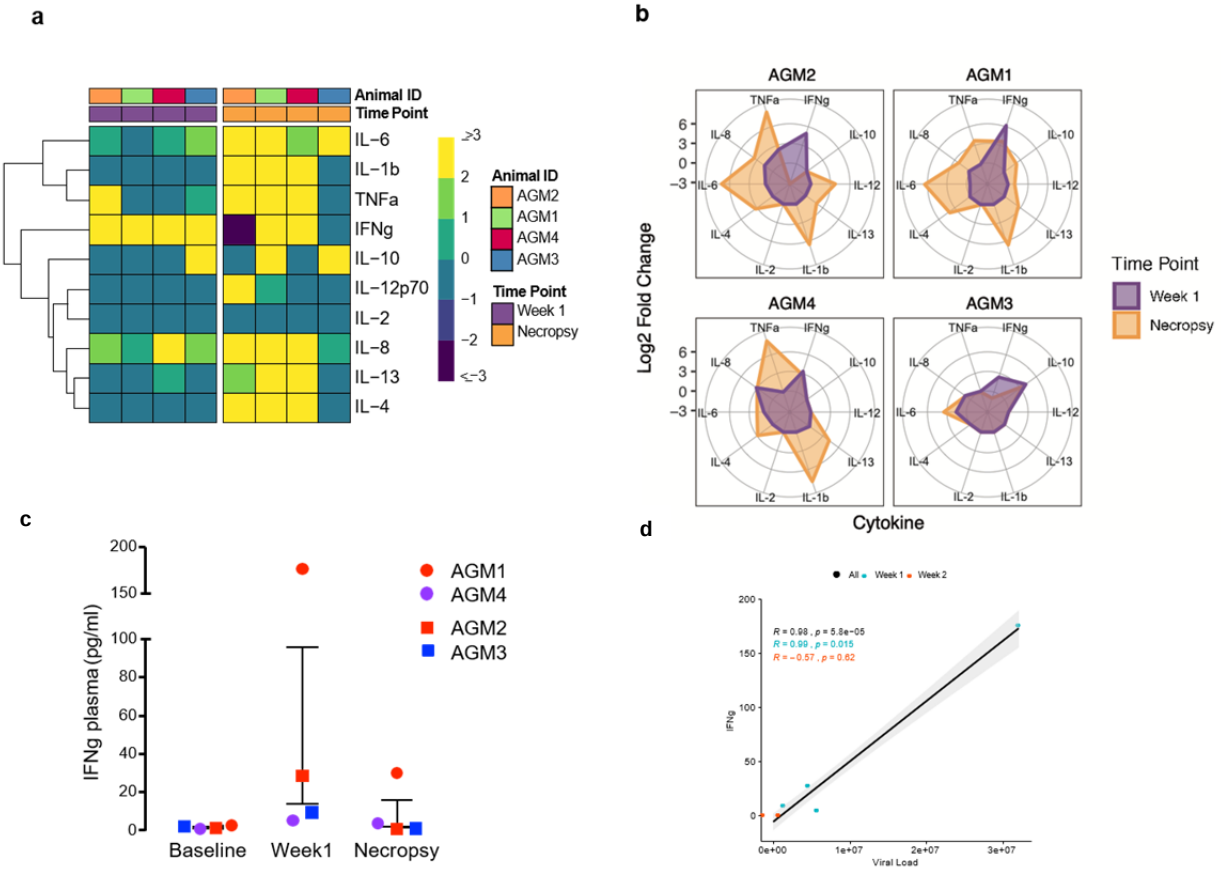

Figure 3 | Cytokine release in SARS-CoV-2 infected AGMs. Heat map (a) and radial plots (b) showing changes in the levels of ten cytokines in plasma at week 1 and necropsy respect to the baseline. Data are normalized (log2). (c) Levels of IFNγ (pg/ml) in plasma at baseline week 1 and at necropsy. (d) Association between IFN levels at week 1 and viral load in bronchiolar brushes (Pearson test with 95% CI). Circles: aerosol exposure; Squares: multiroute exposure; Red: developed ARDS; Purple: cytokine storm without ARDS; Blue: no cytokine storm or ARDS.

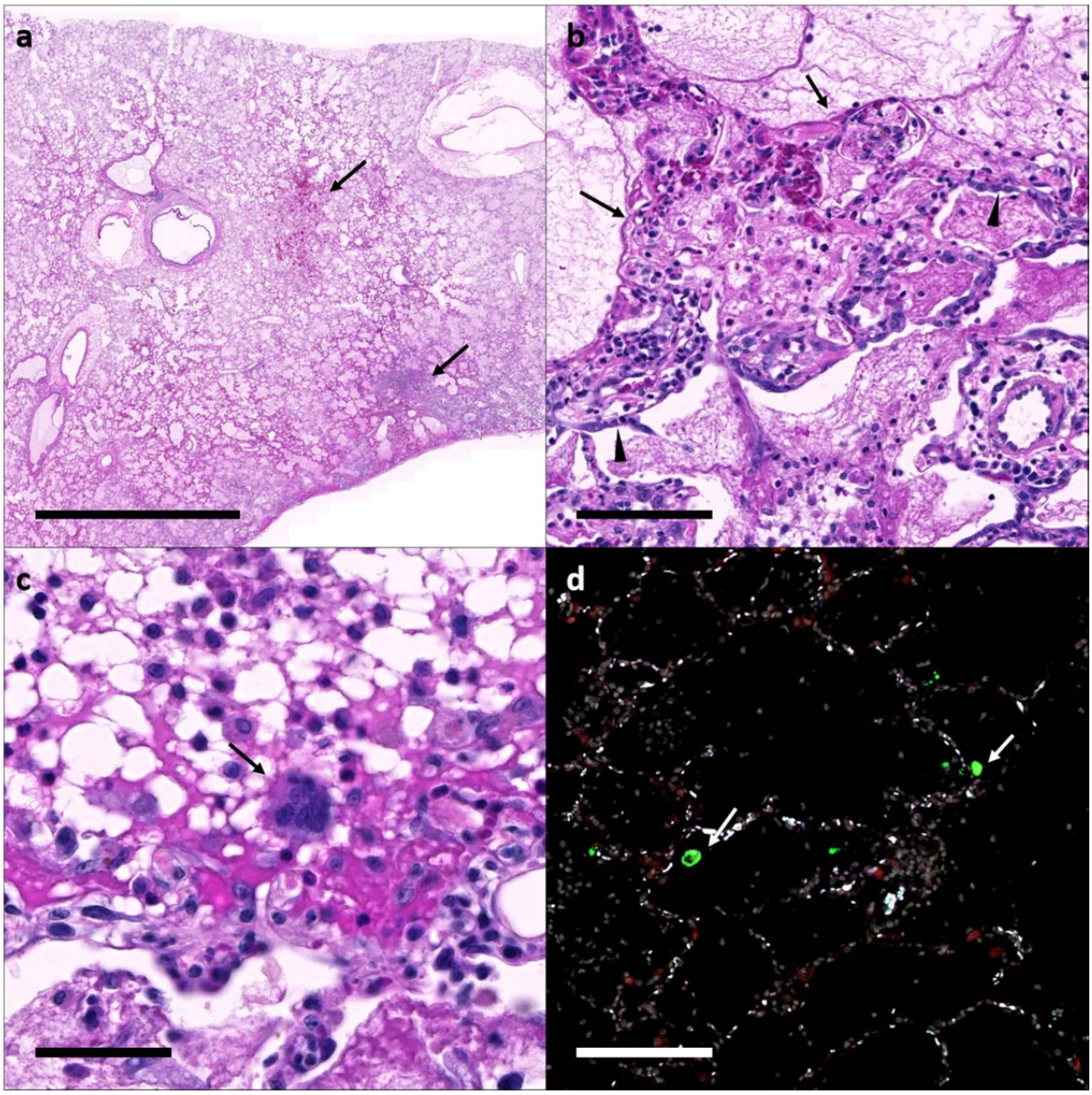

Figure 4 | Histopathology and fluorescent immunohistochemistry in AGM1. (a) The right lower lung lobe is filled with fibrin and edema with areas of hemorrhage and necrosis (arrows); Bar = 5 mm. (b) Alveoli are variably lined by hyaline membranes (arrows) and type II pneumocytes (arrowheads); Bar = 100 um. (c) Rare multinucleated syncytia (arrow) are scattered throughout the affected lungs; Bar = 50 um. (d) Fluorescent immunohistochemistry for COV-2 nucleoprotein (green, arrows) and ACE2 (red) identified low numbers of CoV-2 positive cells within the affected lung lobes; Bar = 100 um. White: DAPI/nuclei; Green: CoV-2; Red: ACE2 Blue: Empty.

Methods

Ethics Statement

The Institutional Animal Care and Use Committee of Tulane University reviewed and approved all the procedures for this experiment. The Tulane National Primate Research Center is fully accredited by the AAALAC. All animals were cared for in accordance with the ILAR Guide for the Care and Use of Laboratory Animals 8th Edition. The Tulane University Institutional Biosafety Committee approved the procedures for sample handling, inactivation, and removal from BSL3 containment.

Virus

The virus used for experimental infection was SARS-CoV-2; 2019-nCoV/USA-WA1/2020 (MN985325.1). Virus stock was prepared in Vero E6 cells and sequence confirmed by PCR and/or Sanger sequencing. Plaque assays were performed in Vero E6 cells.

Animals and procedures

A total of four, aged (≈16 years of age), wild-caught AGM (2M, 2F) were used in this study. Animals (n=2, 1M, 1F) were exposed to SARS-CoV-2 either by small particle aerosol[38] or multiroute combination. The 2 animals (AGM1, AGM4) exposed by aerosol received an inhaled dose of $2.0x10^3$ and $2.5x10^3$ PFU, respectively. AGM2 and AGM3 were exposed by inoculating a cumulative dose of $3.61x10^6$ PFU through multiple routes (oral, 1 mL; nasal, 1mL; intratracheal, 1 mL; conjunctival, 50 µL per eye). Animals were observed for 21 days including twice daily monitoring. Pre- and postexposure samples included blood, CSF, feces, urine, bronchioalveolar lavage, and mucosal swabs (buccal, nasal, pharyngeal, rectal, vaginal, and bronchial brush). Blood was collected at postexposure days -14, 1, 3 (aerosol) or 4 (multiroute), 7, 14, 21, and at necropsy. CSF, feces, urine, bronchioalveolar lavage, and mucosal swabs were collected at postexposure days -14, 7, 14, 21, and at necropsy. Physical exam, plethysmography, and imaging (radiographs and PET/CT) occurred 7 days prior to exposure and then weekly thereafter. Animals were euthanized for necropsy after three weeks postexposure, or when humane end points were reached.

Necropsy

Postmortem examination was performed by a board-certified veterinary pathologist. Blood was collected via intracardiac aspiration. Euthanasia was performed by intracardiac installation of 2 mL of sodium pentobarbital. CSF was collected from the atlanto-occipital space (cisterna magna). Mucosal swabs were collected from the oral cavity, nasal cavity, pharynx, rectum, and vagina. The pluck was removed in its entirety. The left and right lungs were photographed and weighed separately. A bronchial brush was used to sample the mainstem bronchi of the right and left lower lobes. Bronchoalveolar lavage was performed on the right caudal lung lobe. Samples from the left anterior and caudal lung lobes were collected fresh and in media for further processing. All right lung lobes were infused and stored in fixative for microscopic evaluation. The remainder of the necropsy was performed routinely with collection of tissues in media, fixative, or fresh.

Tissue samples were fixed in Z-fix (Anatech), embedded in paraffin and 5 um thick sections were cut, adhered to charged glass slides and stained routinely. Tissue examined microscopically included: nasal turbinate, nasopharynx, trachea, carotid artery, aorta, heart, tongue, salivary gland, esophagus, stomach, duodenum, jejunum, pancreas, ileocecal junction, colon (ascending, transverse, descending), rectum, liver, gall bladder, spleen, kidney, urinary bladder, thyroid, pituitary, adrenal, lymph nodes (bronchial, mesenteric, submandibular, cervical, axillary, inguinal, bronchial), tonsils (palatine, lingual), brain (olfactory bulb, frontal cortex, temporal cortex, parietal cortex, occipital cortex, basal ganglia, cerebellum, brainstem), spinal cord (cervical), and reproductive system (ovary, uterus, vagina or testis, seminal vesicle, prostate).

All slides were scanned on a Zeiss Axio Scan.Z1 digital slide scanner. Images and figures were made using HALO software (Indica Labs).

Quantification of Swab Viral RNA

Swab and bronchial brush samples were collected in 200 µL of DNA/RNA Shield 1x (Cat.# R1200, Zymo Research, Irvine, CA) and extracted for Viral RNA (vRNA) using the Quick-RNA Viral kit (Cat.# R1034/5, Zymo Research). The Viral RNA Buffer was dispensed directly to the swab in the DNA/RNA Shield. A modification to the manufacturers' protocol was made to insert the swab directly into the spin column to centrifugate allowing all the solution to cross the spin column membrane. The vRNA was the eluted (45 µL) from which 5 µL was added in a 0.1 mL fast 96-well optical microtiter plate format (Cat #4346906, Thermo Fisher, CA) for a 20 µL RT-qPCR reaction. The RT-qPCR reaction used TaqPath 1-Step Multiplex Master Mix (Cat.# A28527, Thermo Fisher) along with 2019-nCoV RUO Kit (Cat.# 10006713, IDTDNA, Coralville, IA) a premix of forward and reverse primers and a FAM labeled probe targeting the N1 amplicon of N gene of SARS2-nCoV19 (accession MN908947). The reaction master mix were added using an X-stream repeating pipette (Eppendorf, Hauppauge, NY) to the microtiter plates which were covered with optical film (cat. #4311971; Thermo Fisher), vortexed, and pulse centrifuged. The RT-qPCR reaction was subjected to RT-qPCR a program of, UNG incubation at 25°C for 2 minutes, RT incubation at 50°C for 15 minutes, and an enzyme activation at 95°C for 2 minutes followed by 40 cycles of a denaturing step at 95°C for 3 seconds and annealing at 60°C for 30 seconds. Fluorescence signals were detected with an Applied Biosystems QuantStudio 6 Sequence Detector. Data were captured and analyzed with Sequence Detector Software v1.3 (Applied Biosystems, Foster City, CA). Viral copy numbers were calculated by plotting Cq values obtained from unknown (i.e. test) samples against a standard curve representing known viral copy numbers. The limit of detection of the assay was 10 copies per reaction volume. A 2019-nCoV positive control (Cat.# 10006625, IDTDNA) were analyzed in parallel with every set of test samples to verify that the RT-qPCR master mix and reagents were prepared correctly to produce amplification of the target nucleic acid. A non-template control (NTC) was included in the qPCR to ensure that there was no cross-contamination between reactions.

Immunohistochemistry

5um sections of Formalin-fixed, paraffin-embedded lung were mounted on charged glass slides, baked overnight at 56°C and passed through Xylene, graded ethanol, and double distilled water to remove paraffin and rehydrate tissue sections. A microwave was used for heat induced epitope retrieval. Slides were heated in a high pH solution (Vector Labs H-3301), rinsed in hot water and transferred to a heated low pH solution (Vector Labs H-3300) where they were allowed to cool to room temperature. Sections were washed in a solution of phosphate-buffered saline and fish gelatin (PBS-FSG) and transferred to a humidified chamber. Tissues were blocked with 10% normal goat serum (NGS) for 40 minutes, followed by a 60-minute incubation with the primary antibodies (SARS-CoV-2 nucleoprotein, mouse IgG1 (Sino Biological, cat#40143-MM08); ACE2, rabbit polyclonal (Millipore, cat# HPA000288); Iba-1, rabbit polyclonal (Wako, cat# 019-19741); or pancytokeratin, rabbit polyclonal (Dako, cat#Z0622)) diluted in NGS at a concentration of 1:200 and 1:100, respectively). Slides were washed twice in PBS-FSG with Tritonx100, followed by a third wash in PBS-FSG. Slides were transferred to the humidified chamber and incubated, for 40 minutes, with secondary antibodies tagged with Alexa Fluor fluorochromes and diluted 1:1000 in NGS. Following washes, DAPI (4',6-diamidino-2-phenylindole) was used to label the nuclei of each section. Slides were mounted using a homemade anti-quenching mounting media containing Mowiol (Calbiochem #475904) and DABCO (Sigma #D2522) and imaged with a Zeiss Axio Slide Scanner.

Cytokine Production in Plasma

Plasma was collected by spinning and was thawed before use. Cytokines were measured using Mesoscale Discovery using a V-Plex Proinflammatory Panel 1, 10-Plex (IFN-γ, IL-1β, IL-2, IL-4, IL-6, IL-8, IL-10, IL-12p70, IL-13, TNF-α) (#K15049D, Mesoscale Discovery, Rockville, Maryland) following the instructions of the kit. The plate was read on a MESO Quick Plex SQ120 machine.

Heatmaps were generated using the 'pheatmap' package in R[39,40]. Data were normalized by dividing raw values at week 1 and necropsy by baseline values for each animal, followed by the application of log2. Values below the limit of detection were replaced with the lowest limit of detection value based on the standard curve for each run, or with the lowest value detected during the run, whichever was smaller. Polar coordinate plots were generated using the 'ggplot2' package in R[4140404039], using the same normalized data shown in the heatmap. Scatterplots were drawn using raw data points and display Pearson's correlation coefficients and a 95% confidence interval.

Detection of binding IgG antibody in serum

Serum samples collected at preinfection and at necropsy were tested for binding IgG antibodies against SARS-CoV-2 S1/S2 proteins using an ELISA kit from XpressBio (cat# SP864C). The assays were performed per directions of the manufacturer. In brief, the serum was diluted 1:50 in Sample Diluent. One hundred microliters of diluted serum were pipetted into the wells of the ELISA plate. The plate was covered and incubated at 37° C for 45 min. After incubation, the wells were washed 5 times with 1X wash solution. One hundred microliters of Peroxidase Conjugate were pipetted into each test well. The plate was covered and incubated at 37° C for 45

min. After incubation, the wells were washed 5 times with 1X Wash solution. One hundred microliters of ABTS Peroxidase Substrate was pipetted into each test well. The plate was incubated at room temperature for 30 minutes. The absorbance of the colorimetric reaction was read at 405 nm.

Data Availability

The raw data that supports the findings of this study will be supplied upon request to the corresponding author. Material requests can be made to the Tulane National Primate Research Center. Approved requests for materials will be released after completion of a material transfer agreement. The raw data supporting the findings and figures has been placed in a public data repository which can be accessed here: https://figshare.com/s/0436bb616239b57dc007 and will be made public prior to publication.

Acknowledgements

We would like to acknowledge Natalie Thornburg at the NCIRD for her help acquiring and characterizing the viral stock used in this infection study. We would like to thank the NIH for supporting this work through the TNPRC base grant (P51 OD011104 59).

Author Contributions

RVB lead pathologist and author. MV performed cytokine assay, composed figures, and contributed to writing the manuscript. LADM was the project veterinarian, contributed to study design, and writing of the IACUC and manuscript. CJR conceived and performed aerosol experiments and contributed to writing the manuscript. Kasi Russell-Lodrigue was a project veterinarian, made clinical assessments and collected samples. Marissa Fahlberg analyzed cytokine data and made figures. CJM processed and analyzed samples for RT-qPCR, contributed to writing the manuscript. BB collected and analyzed data. KSP, JAP, SCW provided large preparations of deep sequenced virus from WRCEVA collection. XQ contributed reagents and to the conceptual development of the study. CCM designed IHC panels and performed all the staining. GL contributed to study design, provided administrative support, and aided with sample processing and archiving. NG contributed to study design, study coordination, sample processing, and SOP development. BT, TP contributed to sample processing including RT-qPCR, fluids, swabs, and necropsy tissues. CA analysis and interpretation of antibody data and revision of manuscript. MBB analysis and interpretation of antibody data. MP performed antibody testing. PKD processed and analyzed viral load data. NJM analyzed data and contributed to writing the manuscript. AB reviewed and optimized all technical SOPs and was responsible for safety of this study. TF contributed to study design, planning, and writing of the manuscript. RPB contributed to study design, analysis of clinical and imaging results, and writing the manuscripts. JR conceived, designed, and supported study, analyzed data, contributed to writing the manuscript.

Ethics Declaration

These authors declare no competing interests.

Extended Data.

ID	Species	Source	Age (est. yr)	Sex	Weight (kg)	Exposure (dose)
AGM1	*Chlorocebus aethiops*	Wild caught, St. Kitts	16	F	4.3	Aerosol ($2.0x10^3$PFU)
AGM2	*Chlorocebus aethiops*	Wild caught, St. Kitts	16	F	3.9	Multiroute ($3.61x10^6$ PFU)
AGM3	*Chlorocebus aethiops*	Wild caught, St. Kitts	16	M	6.9	Multiroute ($3.61x10^6$ PFU)
AGM4	*Chlorocebus aethiops*	Wild caught, St. Kitts	16	M	7.5	Aerosol ($2.5x10^3$ PFU)

Extended Data Table 1 | Animal information. Species, source, route and dose of exposure, and demographic information from each animal in the study.

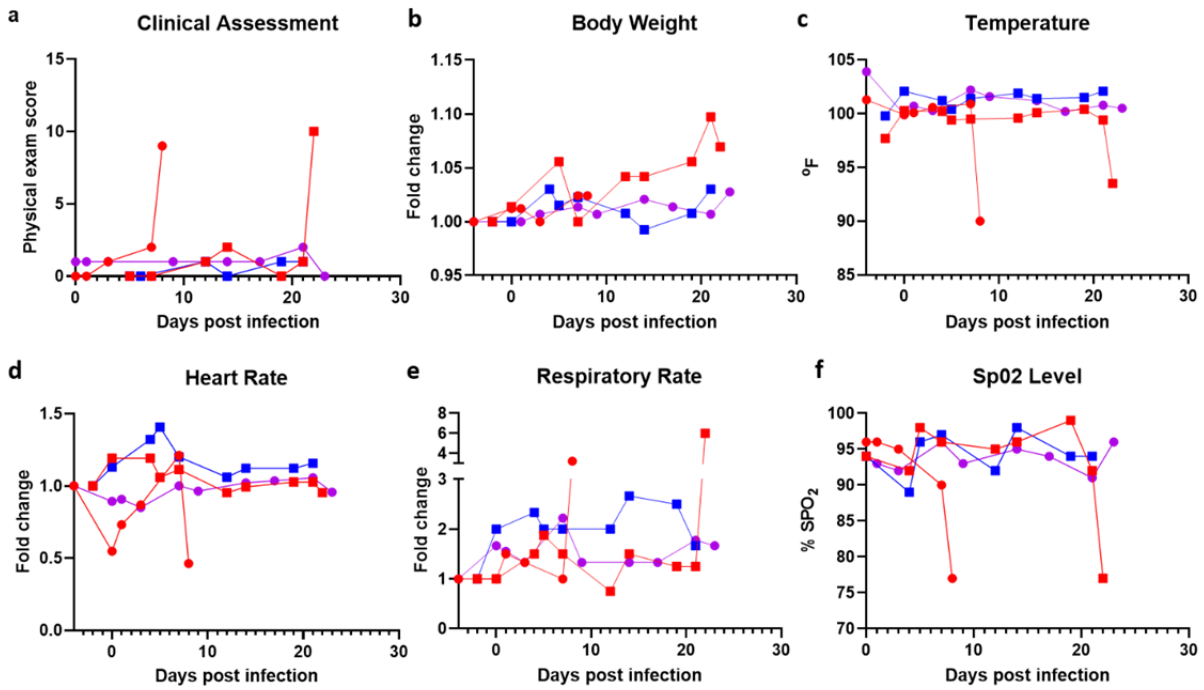

562

563 **Extended Data Figure 1 | Clinical parameters of African Green Monkeys following**
564 **exposure to SARS-CoV-2.** There were no significant differences in clinical parameters leading
565 up to development of ARDS in the two animals that progressed (red). Progression to ARDS was
566 associated with spike in physical exam scores, respiratory rate, and a dramatic decline in SPO2.
567 Neither weight loss nor fever were associated with SARS-CoV-2 exposure in any of the four
568 animals. Circles: aerosol exposure; Squares: multiroute exposure; Red: developed ARDS;
569 Purple: cytokine storm without ARDS; Blue: no cytokine storm or ARDS

570

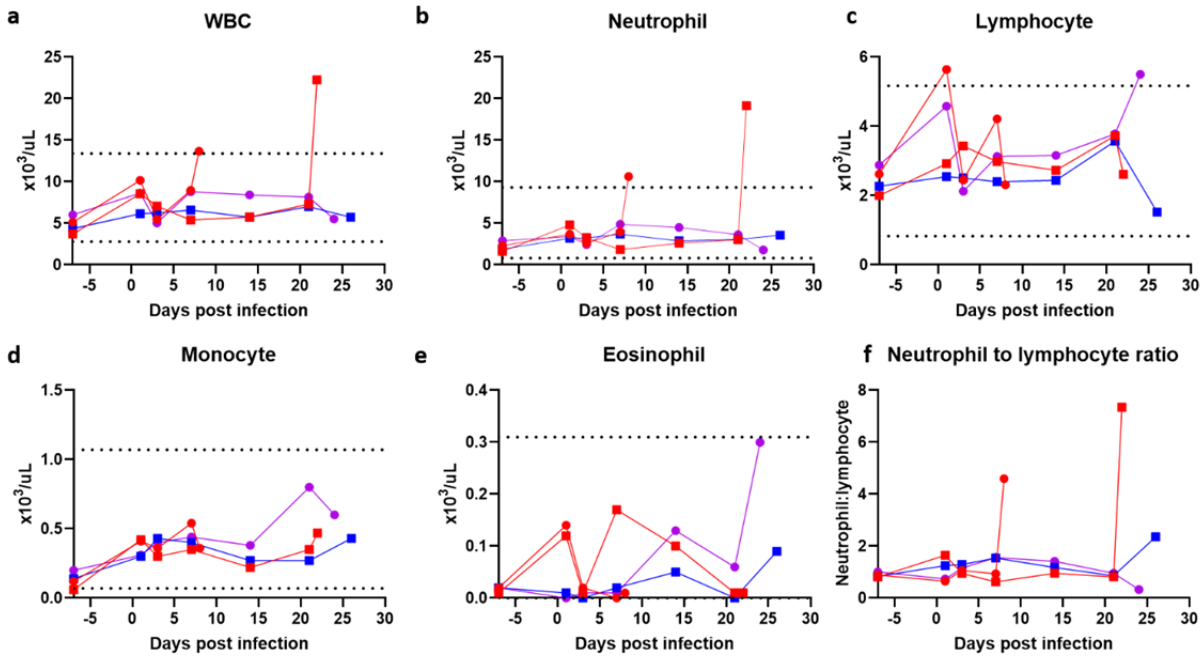

Extended Data Figure 2 | Longitudinal fold changes in leukogram values. The animals that progressed to ARDS (red) did not differ significantly from the nonprogressors (blue and purple), except at terminal timepoints when a spike in WBC, neutrophils, and NLR was observed. All animals exhibited an increase in monocyte numbers from baseline values. Circles: aerosol exposure; Squares: multiroute exposure; Red: developed ARDS; Purple: cytokine storm without ARDS; Blue: no cytokine storm or ARDS. Dashed lines are the upper and lower bounds of the reference range for the parameter.

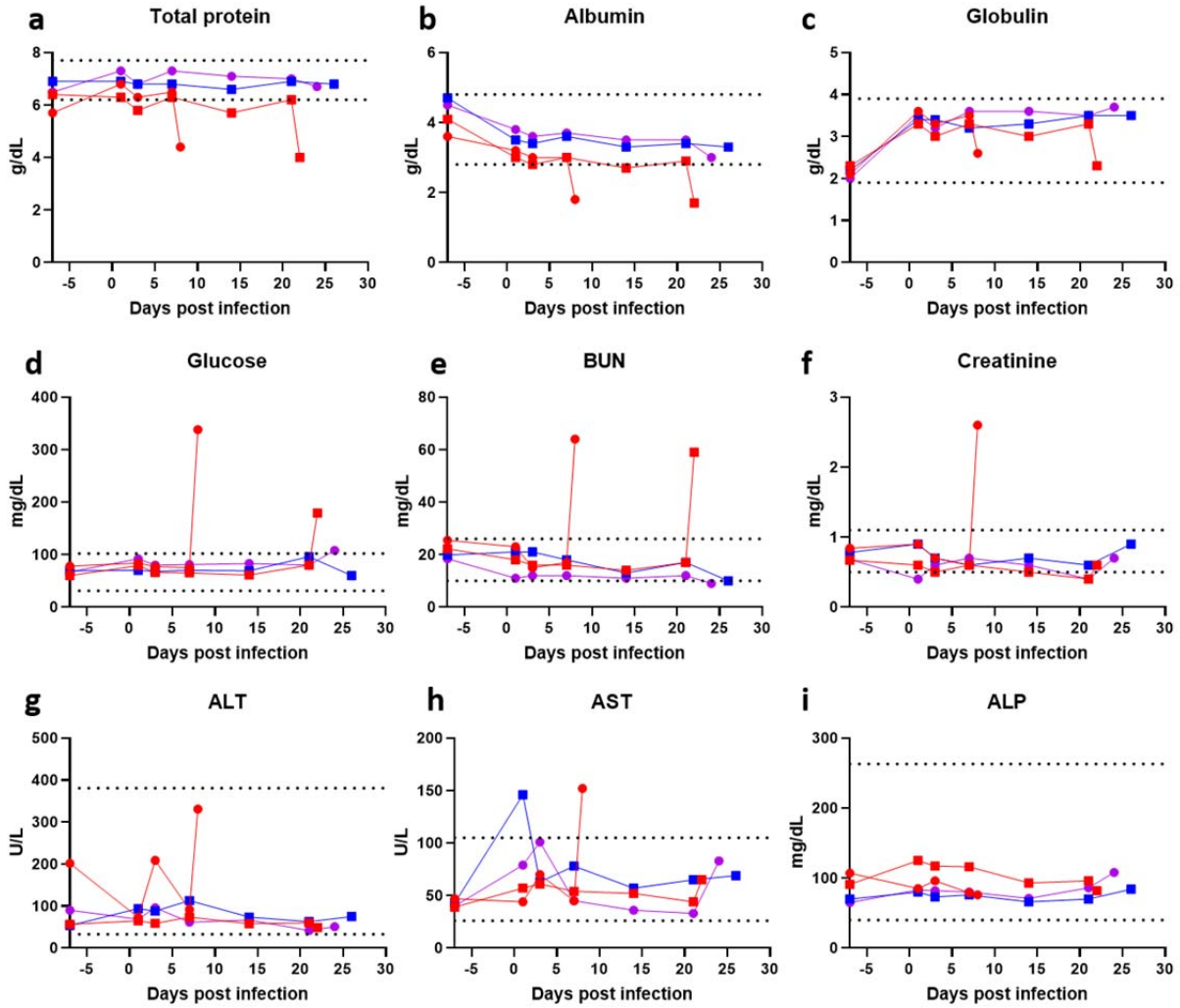

Extended Data Figure 3 | Longitudinal fold changes in serum chemistry values. Animals that progressed to ARDS (red) did not differ significantly from nonprogressors (purple and blue) throughout the course of the study. On the day of necropsy disease progression was associated with a decrease in total protein, albumin, and globulin along with an increase in glucose, blood urea nitrogen, creatinine, and AST in both animals. Circles: aerosol exposure; Squares: multiroute exposure; Red: developed ARDS; Purple: cytokine storm without ARDS; Blue: no cytokine storm or ARDS. Dashed lines are the upper and lower bounds of the reference range for the parameter.

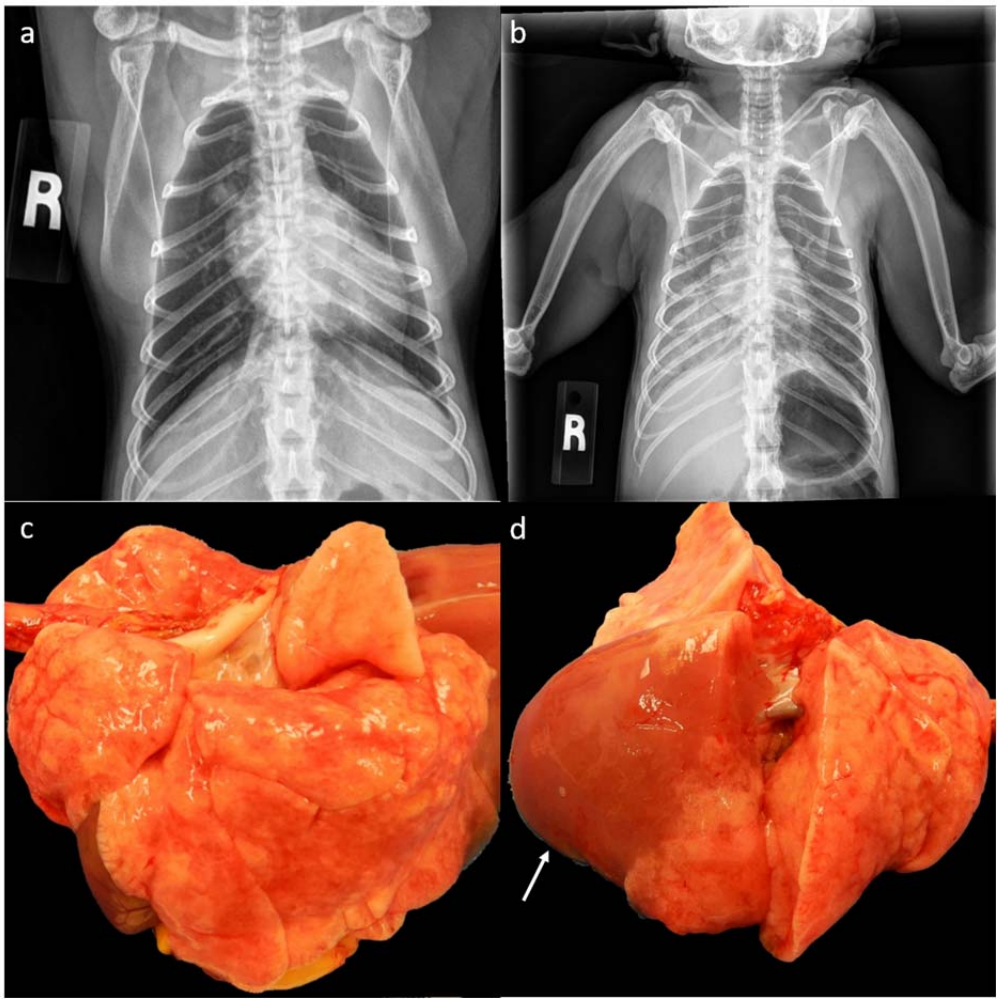

Extended Data Figure 4 | Radiographic and gross pathologic findings of AGM2. Radiographs 24 hours before (a) and at the time of necropsy (b) showing the rapid development of alveolar lung opacities throughout the right lung lobes. (c) The left lung exhibits mild congestion and edema. (d) There is extensive consolidation of the right lower lung lobe with pulmonary edema (arrow). The right middle and anterior lobes are less affected. On cut surface all lobes ooze copious fluid.

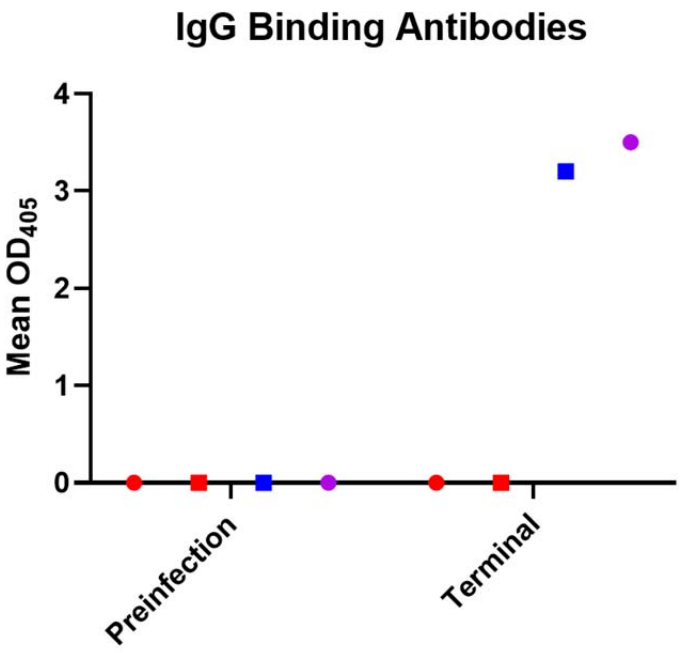

Extended Data Figure 5 | Serum IgG binding antibodies. An ELISA kit was used to detect binding antibodies to SARS-CoV-2 S1/S2 proteins. At terminal timepoints antibodies were not detected in the 2 animals that progressed to ARDS but were detected in the 2 animals that reached study endpoint. None of the animals had detectable antibodies prior to infection. Circles: aerosol exposure; Squares: multiroute exposure; Red: developed ARDS; Purple: cytokine storm without ARDS; Blue: no cytokine storm or ARDS